

Active Phase and Amplitude Fluctuations of Flagellar Beating

Rui Ma,^{1,2} Gary S. Klindt,¹ Ingmar H. Riedel-Kruse,³ Frank Jülicher,¹ and Benjamin M. Friedrich^{1,*}

¹Max Planck Institute for the Physics of Complex Systems, 01187 Dresden, Germany

²Institute for Advanced Study, Tsinghua University, 100084 Beijing, China

³Department of Bioengineering, Stanford University, Stanford, California 94305, USA

(Received 27 January 2014; published 21 July 2014)

The eukaryotic flagellum beats periodically, driven by the oscillatory dynamics of molecular motors, to propel cells and pump fluids. Small but perceivable fluctuations in the beat of individual flagella have physiological implications for synchronization in collections of flagella as well as for hydrodynamic interactions between flagellated swimmers. Here, we characterize phase and amplitude fluctuations of flagellar bending waves using shape mode analysis and limit-cycle reconstruction. We report a quality factor of flagellar oscillations $Q = 38.0 \pm 16.7$ (mean \pm s.e.). Our analysis shows that flagellar fluctuations are dominantly of active origin. Using a minimal model of collective motor oscillations, we demonstrate how the stochastic dynamics of individual motors can give rise to active small-number fluctuations in motor-cytoskeleton systems.

DOI: 10.1103/PhysRevLett.113.048101

PACS numbers: 87.16.Qp, 05.40.Ca, 47.63.Gd, 87.18.Tt

Systems far from equilibrium such as living matter display active, nonthermal fluctuations as well as directed motion and oscillations, which are important for biological function. As a prominent example, molecular motors coupled to cytoskeletal filaments convert chemical energy into work and heat to generate motion at the cellular scale. Motor-filament systems can drive mechanical oscillations including spontaneous hair bundles oscillations in the ear [1], mitotic spindle oscillations during cell division [2], sarcomere oscillations in insect flight muscle [3], and the regular bending waves of cilia and flagella, which propel cells in a liquid including sperm and green algae [4], as well as clear mucus in mammalian airways [5]. Cilia and flagella are slender cell appendages of 10–100 μm length, ubiquitously found in nonbacterial cells, which comprise a conversed cylindrical scaffold of microtubules interspersed by dynein molecular motors.

The collective dynamics of the motors working against a viscoelastic load drives flagellar oscillations via a dynamic instability [6]. Force generation by individual motors relies on the stochastic progression through a mechanicochemical cycle [7]. The stochastic nature of force generation should manifest itself in oscillations that display a characteristic level of noise, representative of active fluctuations. Intriguingly, previous work reported Fourier peaks of finite width in power spectra of flagellar oscillations [8] and phase slips in pairs of synchronized flagella [9–11], which allowed an indirect assessment of flagellar noise. A direct measurement of flagellar fluctuations is pending, let alone a mechanistic understanding. Flagellar fluctuations impart on biological function: Phase fluctuations of flagellar beating should counteract synchronization in collections of flagella, which is important for fast swimming [12] and efficient fluid pumping [13]. Amplitude fluctuations will result in

noisy swimming paths of flagellated swimmers and impart on hydrodynamic interactions between swimmers [14].

Here, we report direct measurements of phase and amplitude fluctuations of the flagellar beat and discuss the microscopic origin of active flagellar fluctuations using a minimal model. We further illustrate the impact of flagellar fluctuations on swimming and synchronization. Our analysis contributes to a recent interest in driven, out-of-equilibrium systems and their fluctuation fingerprint [15–18] by characterizing noisy limit-cycle dynamics in an ubiquitous motility system, the flagellum.

Flagellar shape analysis.—We characterize flagellar beat patterns as the superposition of principal shape modes. This dimensionality reduction is key to our fluctuation analysis. We analyze planar beat patterns of bull sperm swimming close to a boundary surface [19], filmed at 250 frames/s (corresponding to about 8 frames per beat cycle). The flagellar centerline $\mathbf{r}(s, t)$, tracked as function of arclength position s and time t , can be expressed with respect to a material frame of the sperm head in terms of a tangent angle $\psi(s, t)$

$$\mathbf{r}(s, t) = \mathbf{r}_h(t) - \int_0^s ds' [\cos \psi(s', t) \mathbf{e}_1 + \sin \psi(s', t) \mathbf{e}_2]. \quad (1)$$

Here, $\mathbf{r}_h(t)$ denotes the sperm head center, and \mathbf{e}_1 and \mathbf{e}_2 are orthonormal vectors with \mathbf{e}_1 pointing along the long head axis; see Fig. 1(a). A space-time plot of $\psi(s, t)$ reveals the periodicity of the flagellar beat; see Fig. 1(b). This high-dimensional data set can be projected on a low-dimensional “shape space” using shape mode analysis based on principal component analysis [20]. The time-averaged tangent angle $\psi_0(s) = \sum_{i=1}^n \psi(s, t_i)/n$ characterizes the mean

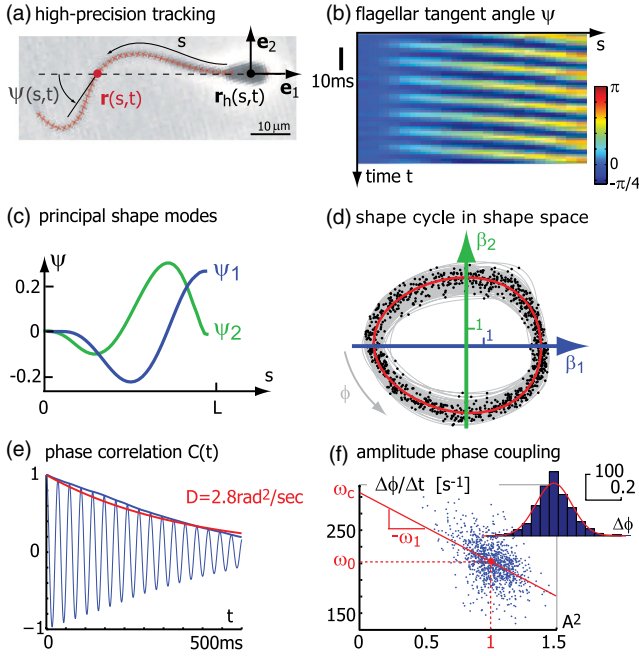


FIG. 1 (color online). The flagellar beat of sperm cells displays active fluctuations. (a) Tracked flagellar shapes are conveniently characterized by a tangent angle $\psi(s, t)$. (b) The kymograph of this tangent angle reveals the periodicity of the flagellar beat. (c) Using principal component analysis, we identify two principal shape modes $\psi_1(s)$, $\psi_2(s)$, whose superpositions account for 95% of the variability of the tangent angle data. (d) By projecting the tangent angle data on the shape space spanned by $\psi_1(s)$ and $\psi_2(s)$, each flagellar shape is assigned a pair of shape coefficients (β_1, β_2) ; see Eq. (2). This representation allows us to define a limit cycle of perfect periodic beating (red). By projection onto this limit cycle, we define a phase φ for each flagellar shape. (e) The flagellar phase-diffusion coefficient D is determined by fitting an exponential decay (red) to the phase correlation function ($|C(t)|$: thick blue, $\text{Re} C(t)$: thin blue). (f) Phase speed $\Delta\varphi/\Delta t$ and squared amplitude $A(t_i)$ are negatively correlated. Inset: phase increments are approximately normally distributed.

shape of the beating flagellum ($n = 1024$ frames in each movie). We further define a two-point correlation matrix $M(s, s') = \sum_i [\psi(s, t_i) - \psi_0(s)][\psi(s', t_i) - \psi_0(s')]$, where s, s' range over m equidistant arclength positions along the flagellum. The eigenvectors $\psi_j(s)$ of the symmetric $m \times m$ -matrix M , sorted by decreasing magnitude of the corresponding eigenvalues, characterize principal shape modes of the flagellar beat. The first two shape modes account for $95 \pm 1\%$ of the variance of the tangent angle data (all measurements are mean \pm s.e., $n = 7$ cells). We project the full data set on a two-dimensional shape space spanned by these two shape modes

$$\psi(s, t) \approx \psi_0(s) + \beta_1(t)\psi_1(s) + \beta_2(t)\psi_2(s) \quad (2)$$

with shape coefficients β_1, β_2 obtained by least-square fit; see Figs. 1(c), 1(d). Flagellar beating implies periodic

shape changes of the flagellum and, thus, noisy oscillations of the shape coefficients with mean frequency $\omega_0 = 2\pi/T$, where $T = 32.4 \pm 1.9$ ms. Individually, $\beta_1(t)\psi_1(s)$ and $\beta_2(t)\psi_2(s)$ describe standing waves; their combination results in a traveling wave propagating from the base to the tip of the flagellum, thereby facilitating net propulsion.

Limit-cycle reconstruction.—The point cloud representing subsequent flagellar shapes in Fig. 1(d) forms a closed loop. This allows us to define a limit cycle of noisy flagellar oscillations (red) by fitting a closed curve $(\bar{\beta}_1(\varphi), \bar{\beta}_2(\varphi))$, parametrized by a phase φ . The phase parametrization of the limit cycle is defined such that the mean of the phase speed is independent of φ [21]. Thus, φ slightly differs from the polar angle in the (β_1, β_2) plane. Next, we assign a unique flagellar phase to each tracked flagellar shape by projecting the corresponding point in the (β_1, β_2) plane radially onto the limit cycle. The shape trajectory $(\beta_1(t), \beta_2(t))$ avoids the singular origin; thus, the instantaneous phase speed $\dot{\varphi}$ is well defined.

Phase fluctuations.—The phase speed $\dot{\varphi}$ has a mean equal to the frequency ω_0 of the beat but can fluctuate around this mean. Phase speed fluctuations cause a decay of the phase-correlation function $C(t) = \langle \exp[i(\varphi(t_0 + t) - \varphi(t_0))] \rangle$; see Fig. 1(e). This decay is insensitive to measurement noise that is uncorrelated from frame to frame. The frame-to-frame phase increments $\Delta\varphi_i = \varphi(t_{i+1}) - \varphi(t_i)$ are approximately normally distributed [Fig. 1(f), inset]. Furthermore, the correlation time of phase speed fluctuations is on the order of our temporal resolution 4 ms or below and, thus, short compared to the time scale of phase decoherence. We can, thus, interpret the observed phase decoherence using an idealized model of δ -correlated phase speed fluctuations,

$$\dot{\varphi} = \omega_0 + \zeta, \quad (3)$$

where ζ is Gaussian white noise with $\langle \zeta(t)\zeta(t') \rangle = 2D\delta(t - t')$ and D denotes a phase-diffusion coefficient. In this idealization, $|C(t)| = \exp(-D|t|)$. By fitting an exponential to measured $|C(t)|$, we obtain the phase-diffusion coefficient of sperm flagellar beating $D = 3.2 \pm 1.9 \text{ s}^{-1}$; see Fig. 1(e). An alternative measure for the phase stability of oscillations is the quality factor, $Q = \omega_0/(2D) = 38.0 \pm 16.7$, where ω_0/Q indicates the width at half-maximum of the principal peak in the power spectral density of $\exp[i\varphi(t)]$.

The observed phase fluctuations of the flagellar beat are dominantly of active origin and surpass passive, thermal fluctuations by orders of magnitude (as suggested by earlier, indirect measurements [10]): For a simple estimate, we consider a flagellar beat that is constrained to move along the shape limit cycle with φ as the only degree of freedom. The friction force P_φ conjugate to φ comprises hydrodynamic friction $\gamma\dot{\varphi}$ and dissipation within the flagellum. We estimate $\gamma \approx 3 \text{ pN}\mu\text{m s}$ [22,23]. We, thus,

obtain an upper bound $k_B T/\gamma \approx 0.0015 \text{ s}^{-1}$ for the contribution of thermal fluctuations to phase diffusion D , which is a thousandfold smaller than the value measured.

Amplitude fluctuations.—We define an instantaneous amplitude of the flagellar beat $A(t) = |\beta_1(t) + i\beta_2(t)|/\rho_0(\varphi(t))$, normalized by $\rho_0(\varphi) = |\beta_1(\varphi) + i\beta_2(\varphi)|$. Thus, the complex oscillator variable $Z(t) = A(t)e^{i\varphi(t)}$ maps the shape limit cycle onto the unit circle. In our data, the amplitude $A(t)$ is approximately normally distributed with $\sigma_A^2 = \langle A(t)^2 \rangle - 1 = 0.0070 \pm 0.0023$ [24]. The autocorrelation function of amplitude fluctuations decays with time constant $\tau_A = 5.9 \pm 1.8 \text{ ms}$. Interestingly, we find that phase speed correlates with amplitude squared; the slope $-\omega_1$ of a linear regression gives $\omega_1/\omega_0 = 0.38 \pm 0.10$; see Fig. 1(f). Thus, the beating flagellum is represented as a nonisochronous oscillator (with approximate isochrones $\varphi - 2\tau_A\omega_1 \ln A = \text{const}$ [25]). Nonisochrony of nonlinear oscillators has been related to synchronization [26,27].

Noisy normal form.—Previous theoretical work described the onset of flagellar oscillations as a supercritical Hopf bifurcation [28] with normal form ($\mu > 0$) [29]

$$\dot{Z} = i(\omega_c - \omega_1|Z|^2)Z + \mu(\Lambda - |Z|^2)Z + \Xi. \quad (4)$$

In the absence of noise $\Xi = 0$ as considered originally [28], the complex oscillator variable $Z(t) = A(t)e^{i\varphi(t)}$ exhibits spontaneous oscillations with amplitude $A = \Lambda^{1/2}$ and frequency $\omega_0 = \omega_c - \omega_1\Lambda$ for effective motor activity $\Lambda > 0$. In this case, we may assume $\Lambda = 1$ after a parameter transformation.

To study the role of fluctuations, we add a multiplicative noise term $\Xi = Z(\zeta_A + i\zeta_\varphi)$ with uncorrelated Gaussian white noise variables satisfying $\langle \zeta_j(t)\zeta_k(t') \rangle = 2D_j\delta_{jk}\delta(t-t')$, $j, k \in \{A, \varphi\}$ and use Stratonovich interpretation. This choice represents the simplest phase-invariant noise term with tunable phase and amplitude noise strengths D_φ and D_A [30]. For weak noise $D_A, D_\varphi \ll \mu\Lambda$, amplitude fluctuations satisfy $\langle A(t_0)A(t_0+t) \rangle - 1 \approx \sigma_A^2 \exp(-|t|/\tau_A)$ with correlation time $\tau_A = (2\mu\Lambda)^{-1}$ and variance $\sigma_A^2 = D_A\tau_A\Lambda$. Phase fluctuations are colored with effective phase-diffusion coefficient $D = D_\varphi + (\omega_1/\mu)^2 D_A$. Our measurements of active flagellar fluctuations, thus, allow the full parametrization of Eq. (4) (with $\Lambda = 1$). Note that in the special case $D_A = D_\varphi \ll \mu\Lambda$ our choice of multiplicative noise gives the same long-term behavior as additive noise.

Flagellar fluctuations imply nondeterministic swimming.—Using measured noise strengths, we simulated realistic beat patterns and corresponding stochastic swimming paths; see Fig. 3(a). Specifically, we (i) use Eq. (4) to simulate $Z(t) = A(t)e^{i\varphi(t)}$, (ii) construct shape coefficients $\beta_1(t) + i\beta_2(t) = A(t)\rho_0(\varphi(t))$ and tangent angles $\psi(s, t)$ by Eq. (2), and (iii) compute the path $\mathbf{r}_h(t)$ using resistive

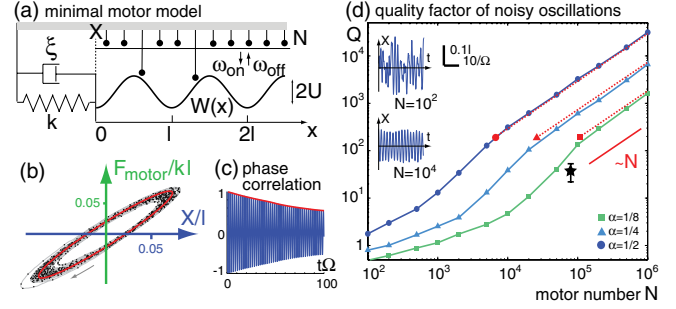


FIG. 2 (color online). A minimal model of coupled motors predicts noisy oscillations. (a) An ensemble of N motors, grafted at a rigid backbone (gray), can bind and unbind to a filament with transition rates ω_{on} and ω_{off} . Bound motors interact with the filament through an interaction potential $W(x)$. Filament and backbone are coupled viscoelastically. (b) The motor model exhibits spontaneous, noisy oscillations, here visualized by filament position X and total motor force. The deterministic limit cycle is shown in red. (c) The phase correlation function $C(t)$ (real part shown in blue) decays exponentially $|C(t)| \approx \exp(-Dt)$, defining the phase-diffusion coefficient D . (d) The quality factor $Q = \omega_0/(2D)$ scales with N for large N , consistent with our analytic approximation (dashed red, Eq. (5)). The star indicates the experimentally measured Q . For all simulations, we chose parameters close to the Hopf bifurcation ($\xi_a/\xi = 1.2\pi^2$, $\nu = 10$, $\alpha = \eta = 0.5$, $N = 10^4$, unless indicated otherwise; errors smaller than symbol size).

force theory [22] as described in Ref. [23]. We find that the center $\mathbf{R}(t)$ of sperm swimming circles diffuses with diffusion coefficient $D_R = 3.3 \mu\text{m}^2/\text{s}$, which is on the same order of magnitude, albeit smaller, than a value $D_R = 9 \pm 2 \mu\text{m}^2/\text{s}$ measured for sea urchin sperm [8]. Our analysis includes amplitude and phase fluctuations but neglects additional shape fluctuations; thus, our value is a lower bound.

Although phase and amplitude fluctuations are correlated, we can ask separately for their respective effect on swimming. Phase fluctuations cause fluctuations in swimming speed but do not change the shape of the path. This is because the Stokes equation governing self-propulsion at low Reynolds numbers [31] is invariant under (stochastic) reparametrizations of time.

To gain qualitative insight into the microscopic origin of noisy oscillations and the dependence of phase diffusion on microscopic parameters, we now discuss a minimal motor model and show how it can be mapped onto Eq. (4).

A minimal model for noisy motor oscillations.—We exemplify how a finite collection of motors drives spontaneous oscillations with characteristic small-number fluctuations using the classical two-state model [6,32] in its most simple form: A collection of N motors, rigidly attached to an inextensible backbone interacts with a filament through an effective potential $W(x) = U[1 - \cos(2\pi x/l)]$; see Fig. 2(a). Here, x is the coordinate of the motor along the filament, and l is the periodicity of the filament. Individual motors

can bind to and unbind from the filament with rates $\omega_{\text{on}}(x) = \Omega[\eta - \alpha \cos(2\pi x/l)]$ and $\omega_{\text{off}} = \Omega - \omega_{\text{on}}$. Here, η denotes the mean fraction of attached motors (“duty ratio”). Importantly, the binding rates are spatially inhomogeneous, characterized by α , and break detailed balance. If the filament is now coupled to the backbone by a viscoelastic element with viscosity ξ and elastic stiffness k , we obtain a force-balance equation for the position $X(t)$ of the filament $kX + \xi\dot{X} = F_m$ with $F_m = -\sum_i \partial_x W(x_i - X)$, where the sum extends over all bound motors and $x_i = il/N$ is a simple choice for the positions of the motors along the backbone.

To properly define a thermodynamic limit for large N , we rescale stiffness and viscosity as $k = k_0 N$ and $\xi = \xi_0 N$. In the limit $N \rightarrow \infty$, the system can exhibit spontaneous oscillations by a supercritical Hopf bifurcation, when the normalized motor activity $\xi_a/\xi = 2\pi^2\alpha U/(\Omega l^2 \xi_0)$ exceeds the threshold $1 + \nu$, where $\nu = k/(\xi\Omega)$ [32]. For a finite motor number, we numerically observe noisy oscillations; see Fig. 2.

In the following, we analytically compute the quality factor Q in the limit of large (yet finite) motor number N , assuming that we are close to the Hopf bifurcation with $\varepsilon = \xi_a/\xi - 1 - \nu$ positive and small. Following Refs. [32,33], we first approximated the stochastic binding and unbinding dynamics of individual motors by a diffusion approximation, thus arriving at a Fokker-Planck equation for the probability distribution of filament position and density $\rho(x)$ of bound motors (see Supplemental Material [34] for details). Because of the simple choice of potential $W(x)$, the dynamics of the first Fourier mode of $\rho(x)$ decouples from that of the higher modes, resulting in a three-dimensional stochastic system [33]. A nonlinear coordinate transformation maps this system onto Hopf normal form Eq. (4), with oscillator variable Z satisfying $\text{Re } Z = X/l + \mathcal{O}(\varepsilon^{3/2})$ and phase-dependent noise term $\Xi = i\zeta$, where $\langle \zeta(t)\zeta(t') \rangle = 4D\Lambda\delta(t-t')$. The quality factor $Q = \omega_0/(2D)$ is found to scale with N

$$Q \approx \frac{\omega_0}{2\Omega\eta(1-\eta)} \left(\frac{2\pi\alpha}{\sqrt{\nu} + 1/\sqrt{\nu}} \right)^2. \quad (5)$$

Furthermore, $\Lambda \approx \varepsilon(1+4\nu)/[3\pi^2\nu(1+2\nu)]$, $\mu \approx \Omega\varepsilon/(2\Lambda)$, $\omega_0 \approx \Omega\sqrt{\nu}[1 + \varepsilon/(2+4\nu)]$. Interestingly, the motor duty ratio η controls oscillation quality, although η affects neither amplitude nor frequency (for $N \rightarrow \infty$). To understand this, note that the number of bound motors fluctuates with mean ηN and variance $\eta(1-\eta)N$. This number characterizes a spatially homogeneous “background” of bound motors, which does not contribute directly to the oscillations but sets the amplitude of motor density fluctuations responsible for phase diffusion. Oscillations become also more regular for increasing amplitude. Equation (5) and simulations of the full model agree well close to the Hopf bifurcation; see Fig. 2. This minimal

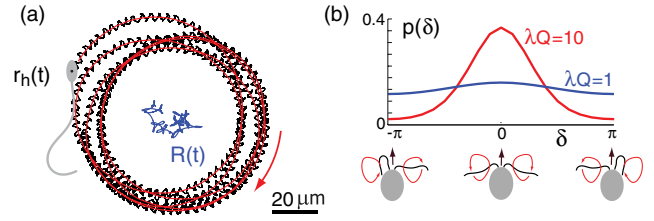


FIG. 3 (color online). Flagellar fluctuations imply nondeterministic swimming and counteract synchronization. (a) We simulated stochastic sperm swimming paths $r_h(t)$ (black), using measured flagellar fluctuation strengths. Fluctuations imply that the blue center $R(t)$ of red sperm swimming circles diffuses, with apparent diffusion coefficient $D_R = 3.30 \pm 0.01 \mu\text{m}^2/\text{s}$. (b) Pairs of flagella can synchronize, e.g., in the green alga *Chlamydomonas*. In a simple description of flagellar synchronization, the phase difference δ between its two flagella peaks around zero for realistic noise strength ($\lambda Q = 10$) but is almost uniformly distributed for tenfold stronger noise ($\lambda Q = 1$), indicating lack of synchronization.

motor model recapitulates the experimental observation of phase diffusion in a minimal setting and illustrates how noisy oscillations can arise from small-number fluctuations.

Flagellar synchronization.—Phase fluctuations cause phase slips in pairs of synchronized flagella, e.g., in the green algae *Chlamydomonas* [10]. *Chlamydomonas* swims with two flagella, which can synchronize their beat. Analysis of phase slips allowed a previous, indirect estimate of flagellar phase fluctuations, corresponding to $Q \approx 25$ for the quality factor of individual flagella [10]. A latter study indicated a length dependence of Q , with corresponding Q ranging from ≈ 70 – 120 for length increasing from 6 to 12 μm [35]. Interestingly, flagellar synchronization in *Chlamydomonas* seems to operate just below a tolerable level of noise: Consider the approximate dynamics of the phase difference δ between two identical, coupled oscillators $\dot{\delta} = -\lambda/T \sin \delta + \zeta$, where ζ is Gaussian white noise with $\langle \zeta(t)\zeta(t') \rangle = 4D\delta(t-t')$ [10,36]. Using the estimate $\lambda \approx 0.3$ for the synchronization strength [10], we find $\lambda Q \approx 10$, which yields robust synchronization. A tenfold higher noise level, however, implies failure of synchronization; see Fig. 3(b).

Conclusion.—The beating flagellum is a noisy oscillator, driven by $N \approx 8 \times 10^4$ dynein motor domains [37]. Here, we precisely measured its phase and amplitude fluctuations, using a novel method of limit-cycle reconstruction [20]. We obtain a quality factor $Q = 38 \pm 16.7$ of flagellar oscillations. Values estimated in other cytoskeletal oscillators are $Q = 2.2 \pm 1.0$ ($N \approx 2500$) for spontaneous hair bundle oscillations [38] and $Q = 1.4 \pm 1.1$ ($N = 10$ – 100) for an *in vitro* acto-myosin system [16]. We find that the strength of flagellar phase fluctuations is several orders of magnitudes above the level corresponding to thermal noise, highlighting the active origin of flagellar fluctuations.

We compute the quality factor Q in a minimal model of motor-filament oscillations and find that Q is proportional to the number of motors. A simple numerical example [39] yields noisy oscillations with amplitude, frequency, and quality factor $Al \approx 68$ nm, $\omega_0 \approx 228$ s⁻¹, $Q \approx 33$, which roughly match measured values ($Al \approx 100$ nm, $\omega_0 \approx 200$ s⁻¹ [19], $Q \approx 38$). Our analytic approximation Eq. (5) is not applicable for these large-amplitude oscillations. Note that the model does not fully capture flagellar oscillations quantitatively because it strongly simplifies flagellar geometry and motor dynamics.

We show that phase and amplitude fluctuations affect sperm swimming differently: Whereas amplitude fluctuations cause an effective diffusion of sperm swimming circles, phase fluctuations imply speed fluctuations but do not change the shape of the path. Additionally, phase fluctuations introduce phase slips in collections of synchronized flagella [10].

We thank J. Baumgart, V.F. Geyer, J. Howard, P. Romanczuk, P. Sartori, and T. Schwalger for stimulating discussions. Experimental data were recorded previously by I. H. Riedel-Kruse in the laboratory of J. Howard. We gratefully acknowledge support within the DFG priority program SPP 1726 “Microswimmers” (FR 3429/1-1).

*benjamin.friedrich@pks.mpg.de

- [1] P. Martin, D. Bozovic, Y. Choe, and A.J. Hudspeth, *J. Neurosci.* **23**, 4533 (2003).
- [2] S. W. Grill, K. Kruse, and F. Jülicher, *Phys. Rev. Lett.* **94**, 108104 (2005).
- [3] B. Jewell and J. Ruegg, *Proc. R. Soc. B* **164**, 428 (1966).
- [4] J. Gray, *Ciliary Movements* (Cambridge University Press, Cambridge, England, 1928).
- [5] M.J. Sanderson and M. A. Sleight, *J. Cell Sci.* **47**, 331 (1981).
- [6] F. Jülicher and J. Prost, *Phys. Rev. Lett.* **78**, 4510 (1997).
- [7] J. Howard, *Mechanics of Motor Proteins and the Cytoskeleton* (Sinauer, Sunderland, MA, 2001).
- [8] I. H. Riedel, K. Kruse, and J. Howard, *Science* **309**, 300 (2005).
- [9] M. Polin, I. Tuval, K. Drescher, J. P. Gollub, and R. E. Goldstein, *Science* **325**, 487 (2009).
- [10] R. E. Goldstein, M. Polin, and I. Tuval, *Phys. Rev. Lett.* **103**, 168103 (2009).
- [11] K. Y. Wan, K. C. Leptos, and R. E. Goldstein, *J. R. Soc. Interface* **11**, 20131160 (2014).
- [12] C. Brennen and H. Winet, *Annu. Rev. Fluid Mech.* **9**, 339 (1977).
- [13] N. Osterman and A. Vilfan, *Proc. Natl. Acad. Sci. U.S.A.* **108**, 15727 (2011).
- [14] K. Drescher, J. Dunkel, L. H. Cisneros, S. Ganguly, and R. E. Goldstein, *Proc. Natl. Acad. Sci. U.S.A.* **108**, 10940 (2011).
- [15] T. Betz, M. Lenz, J.-F. Joanny, and C. Sykes, *Proc. Natl. Acad. Sci. U.S.A.* **106**, 15320 (2009).
- [16] P.-Y. Plaçais, M. Balland, T. Guérin, J.-F. Joanny, and P. Martin, *Phys. Rev. Lett.* **103**, 158102 (2009).
- [17] E. Ben-Isaac, Y. Park, G. Popescu, F. L. H. Brown, N. S. Gov, and Y. Shokef, *Phys. Rev. Lett.* **106**, 238103 (2011).
- [18] M. Otten, A. Nandi, D. Arcizet, M. Gorelashvili, B. Lindner, and D. Heinrich, *Biophys. J.* **102**, 758 (2012).
- [19] I. H. Riedel-Kruse, A. Hilfinger, J. Howard, and F. Jülicher, *HFSP J.* **1**, 192 (2007).
- [20] V. F. Geyer, F. Jülicher, J. Howard, and B. M. Friedrich, *Proc. Natl. Acad. Sci. U.S.A.* **110**, 18058 (2013).
- [21] B. Kralemann, L. Cimponeriu, M. Rosenblum, A. Pikovsky, and R. Mrowka, *Phys. Rev. E* **77**, 066205 (2008).
- [22] J. Gray and G. T. Hancock, *J. Exp. Biol.* **32**, 802 (1955).
- [23] B. M. Friedrich, I. H. Riedel-Kruse, J. Howard, and F. Jülicher, *J. Exp. Biol.* **213**, 1226 (2010).
- [24] The contribution from measurement noise is small. As a test, we added random perturbations to $\mathbf{r}(s, t)$, using known accuracies of tracking [19]. Phases and amplitudes for perturbed and unperturbed data were strongly correlated; results for σ_A did not significantly change.
- [25] A. Pikovsky, M. Rosenblum, and J. Kurths, *Synchronization* (Cambridge University Press, Cambridge, England, 2001).
- [26] T. Niedermayer, B. Eckhardt, and P. Lenz, *Chaos* **18**, 037128 (2008).
- [27] M. Leoni and T. B. Liverpool, *Phys. Rev. E* **85**, 040901 (2012).
- [28] S. Camalet and F. Jülicher, *New J. Phys.* **2** (2000).
- [29] J. Crawford, *Rev. Mod. Phys.* **63**, 991 (1991).
- [30] R. Graham, *Phys. Rev. A* **25**, 3234 (1982).
- [31] E. Lauga and T. R. Powers, *Rep. Prog. Phys.* **72**, 096601 (2009).
- [32] T. Guérin, J. Prost, and J.-F. Joanny, *Eur. Phys. J. E* **34** (2011).
- [33] T. Guérin, J. Prost, and J.-F. Joanny, *Phys. Rev. E* **84**, 041901 (2011).
- [34] See Supplemental Material at <http://link.aps.org/supplemental/10.1103/PhysRevLett.113.048101> for additional details on the derivation of Eq. (5).
- [35] R. E. Goldstein, M. Polin, and I. Tuval, *Phys. Rev. Lett.* **107**, 148103 (2011).
- [36] R. L. Stratonovich, *Topics in the Theory of Random Noise* (Gordon and Breach, New York, 1963).
- [37] D. Nicastro, C. Schwartz, J. Pierson, R. Gaudette, M. E. Porter, and J. R. McIntosh, *Science* **313**, 944 (2006).
- [38] J. Barral, K. Dierkes, B. Lindner, F. Jülicher, and P. Martin, *Proc. Natl. Acad. Sci. U.S.A.* **107**, 8079 (2010).
- [39] $N = 8 \times 10^4$, $l = 8$ nm, $k \approx 2$ nN/ μ m [7], $\xi \approx 40$ pN/ μ m, $\Omega = 10^4$ s⁻¹, $\xi_a/\xi = 2$, $\alpha = \eta = 0.5$.